Ballistic Electron Transport in AlAs Quantum Wells

O. Gunawan, Y. P. Shkolnikov, E. P. De Poortere, E. Tutuc, and M. Shayegan
Department of Electrical Engineering, Princeton University, Princeton, New Jersey 08544, USA
(Received 2 February 2004; published 8 December 2004)

We report the observation of commensurability oscillations in an AlAs two-dimensional electron system where two conduction-band valleys with elliptical in-plane Fermi contours are occupied. The Fourier power spectrum of the oscillations shows two frequency components consistent with those expected for the Fermi contours of the two valleys. From an analysis of the spectra we deduce $m_l/m_t = 5.2 \pm 0.5$ for the ratio of the longitudinal and transverse electron effective masses, a fundamental parameter that cannot be directly measured from other transport experiments.

DOI: 10.1103/PhysRevLett.93.246603 PACS numbers: 72.20.–i, 73.23.Ad, 75.47.Jn

Electrons confined to a modulation-doped AlAs quantum well are an emerging, high-mobility, two-dimensional electron system (2DES) with some unique properties that are very different from those of the more commonly studied GaAs 2DES [1–3]. AlAs 2D electrons occupy multiple valleys in the conduction-band, each with a large and anisotropic effective mass, and possess a much larger effective g factor than GaAs 2D electrons. The combination of these properties has led to the observation of new phenomena in AlAs 2DES. Examples include magnetic phase transitions, marked by sharp resistance spikes, at Landau level crossings in tilted magnetic fields [3], and fractional quantum Hall states at very high Landau level filling factors, stabilized possibly because of the multivalley occupancy [1]. Here we report measurements of commensurability oscillations (COs) in a high-mobility AlAs 2DES subjected to a one-dimensional, lateral, periodic potential modulation. The electrons in our system occupy two valleys with elliptical in-plane Fermi contours. The results demonstrate ballistic transport in a two-valley 2DES. Through Fourier and partial inverse Fourier analyses of the oscillations, we disentangle and study the COs of the electrons in the two valleys, and obtain their amplitude, phase and scattering time. More importantly, from an analysis of the CO frequencies, we directly determine the ratio of the longitudinal and transverse electron effective masses.

In bulk AlAs, electrons occupy conduction-band valleys centered at the six equivalent X points of the Brillouin zone. The Fermi surface consists of six, anisotropic, half-ellipsoids (three full-ellipsoids); we denote these ellipsoids (valleys) by X, Y, and Z, according to the direction of their major axes (x, y, and z). In a narrow (< 5 nm wide) AlAs quantum well grown on a GaAs (001) substrate, thanks to its larger mass in the confinement direction, the Z valley (out-of-plane valley) has the lowest energy and is occupied by electrons. For wider well widths, however, the strain from the lattice mismatch between GaAs and AlAs pushes the X and Y valleys (the in-plane valleys) down in energy with respect to the Z valley, so that now the X and Y valleys are occupied [4–8]. This is the case for the samples we have studied.

Figure 1 highlights the basic principle of our study. Using a grated surface gate, we apply a lateral periodic potential with period a to the 2DES, and measure the low-field magnetoresistance (ρ_{xx}) along the potential modulation direction as a function of a perpendicular magnetic field B. If transport is ballistic, ρ_{xx} oscillates with B as the classical electron cyclotron orbit diameter takes on values that are multiple integers of a [9–13]:

$$\rho_{xx} \propto \cos(2\pi f_{\mathrm{CO}}/B - \pi/2), \tag{1}$$

$$f_{\mathrm{CO}} = 2\hbar k_F/ea, \tag{2}$$

where f_{CO} is the oscillation frequency and k_F is the Fermi wave vector perpendicular to the modulation direction (parallel to the grating stripes). Note that the oscillations are periodic in $1/B$. In our AlAs 2DES, there are two in-plane valleys occupied: X and Y. Their cyclotron orbits in real space have the same shape as their k space orbits but rotated by 90° as shown in Fig. 1(b). If both valleys participate in the ballistic transport independently, we

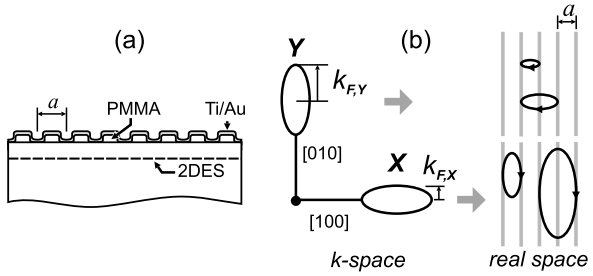

FIG. 1. (a) Schematic cross section of the device used to measure COs. Application of a bias to the Ti/Au surface gate with respect to the 2DES produces a potential modulation which is periodic in the [100] direction and has period a. (b) The AlAs in-plane valleys X and Y in k space (left), and their corresponding first two resonant CO orbits in real space (right) [13]. The Fermi wave vectors $k_{F,X}$ and $k_{F,Y}$ relevant for the COs of the X and Y valley are also indicated.

expect two superimposed sets of COs whose frequencies are related to the Fermi wave vectors parallel to the grating stripes as indicated in Fig. 1(b):

$$k_{F,X}^2 = 2\pi n_X \sqrt{m_t/m_l}, \qquad k_{F,Y}^2 = 2\pi n_Y \sqrt{m_l/m_t}, \quad (3)$$

where n_X and n_Y are the 2D electron densities for the X and Y valleys, respectively. These relations can be combined to yield

$$m_l/m_t = (f_{\mathrm{CO},Y}/f_{\mathrm{CO},X})^2 (n_X/n_Y) \quad (4)$$

implying that, if the valley densities are known, the frequencies of the COs can be used to directly determine the mass anisotropy ratio m_l/m_t, independent of a.

We used samples grown by molecular beam epitaxy on (001) GaAs substrates [1]. The 2DES is confined in an 11 nm-wide AlAs layer located at 110 nm below the surface and sandwiched between barrier layers of $Al_{0.4}Ga_{0.6}As$. It is modulation-doped with a Si delta layer placed at a distance of 75 nm away. A 20 μm Hall bar mesa, with voltage probes 25 μm apart, was defined on each sample using standard photolithography and wet etching techniques. The Hall bar was aligned along the [100] direction so that the major axes of the two in-plane valleys were either parallel or perpendicular to the Hall bar. To fabricate the grating patterns, we spun 150 nm of polymethylmetacrylate (PMMA) on top of the sample, and used electron beam lithography to define arrays of PMMA ridges with periods a equal to 300 and 400 nm and widths equal to $a/2$. We then deposited 10 nm Ti and 30 nm Au to form a top gate. Each section of the Hall bar was entirely covered by the PMMA ridge array and the top gate. Biasing this top gate with respect to the 2DES changes the 2DES density and also results in a periodic potential modulation in the 2DES. We varied the 2DES density between 5 and 9×10^{11} cm^{-2} by applying a bias of 0.5 to 2.2 V [14]. The typical low-temperature mobility in our samples is $\sim$10 m^2/V s prior to patterning the grating, and $\sim$3 m^2/V s after the patterning. The mean-free path deduced from these mobilities is $\sim$1 μm; this is of the order of the grating period in our samples, consistent with our observation of (ballistic) COs. We measured ρ_{xx} in a ^{3}He cryostat with a base temperature of 0.35 K, and used a standard lock-in technique.

A typical ρ_{xx} vs B trace, taken at a total density $n_{\mathrm{tot}} = 8.7 \times 10^{11}$ cm^{-2}, is shown in Fig. 2(a). It exhibits both COs, in the low-field range $-1 < B < 1$ T, and Shubnikov–de Haas oscillations (SdHOs), at $B > 1.7$ T. The COs are more clearly seen in the second derivative ($d^2\rho_{xx}/dB^2$) plot shown in the inset of Fig. 2(a). Fortunately, the COs and SdHOs are well separated in their field range, thus simplifying their analysis.

The SdHOs provide information regarding the electron densities of the 2DES and the valleys. In Fig. 2(c) we show the Fourier power spectrum of the SdHOs. To calculate this spectrum, we used the ρ_{xx} vs $1/B$ data for $B > 1.7$ T, subtracted a second-order polynomial background, and multiplied the data by a Hamming window [15] in order to reduce the side-lobes in the spectrum. The spectrum exhibits three peaks, marked in Fig. 2(c) as n_{tot}, $n_{\mathrm{tot}}/2$, and $n_{\mathrm{tot}}/4$. The peak frequencies multiplied by e/h give the 2D density (e is the electron charge and h is the Planck's constant). We associate the n_{tot} peak with the total density, as this peak's frequency multiplied by e/h indeed gives the total 2DES density which we independently determine from the Hall coefficient. For Fig. 2 data, we deduce $n_{\mathrm{tot}} = n_X + n_Y = 8.7 \times 10^{11}$ cm^{-2}. The presence of the $n_{\mathrm{tot}}/4$ peak indicates the spin and valley degeneracy of the 2DES [16].

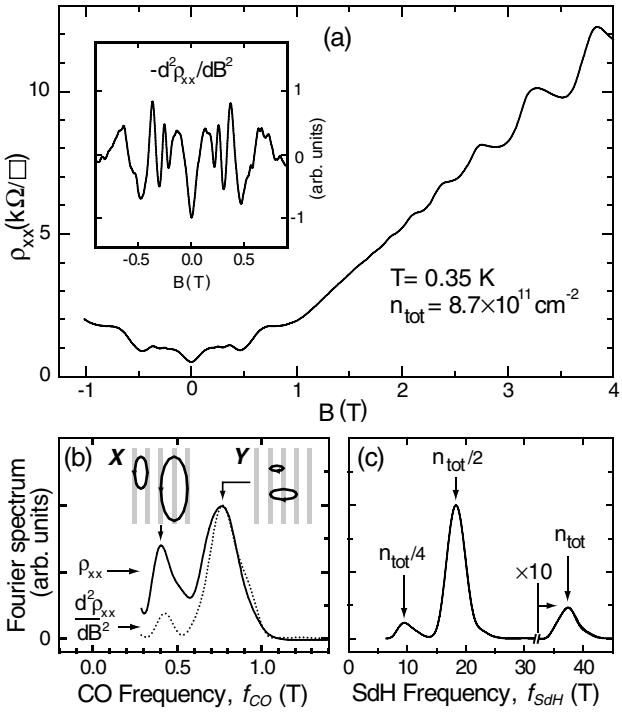

FIG. 2. (a) Magnetoresistance trace showing COs at low fields ($-1 < B < 1$ T) and SdHOs at high fields ($B > 1.7$ T) for a device with 400 nm grating period. Inset: numerically determined second derivative $d^2\rho_{xx}/dB^2$. (b) Fourier power spectra of COs from both ρ_{xx} (solid curve) and $d^2\rho_{xx}/dB^2$ (dotted curve). (c) Fourier power spectrum of SdHOs.

Figure 2(b) shows the Fourier power spectra of COs calculated using ρ_{xx} and $d^2\rho_{xx}/dB^2$ vs $1/B$ data in the $0.1 < B < 1$ T range. Both spectra exhibit two clear peaks at $f_{\mathrm{CO},X}$ and $f_{\mathrm{CO},Y}$, which we associate with the CO frequencies of the X and Y valleys, respectively. If we assume that the two valleys have equal densities, we can use Eq. (4) to immediately find $m_l/m_t \simeq 4.4$. This value, however, is inaccurate because there is a small but finite imbalance between the X and Y valley densities in our sample. Such imbalances can occur because of anisotropic strain in the plane of the sample and are very often present in AlAs 2DESs [1–8]. Note that the Fourier spectrum of the SdHOs cannot resolve small valley density imbalances. As detailed in the next paragraph, we analyze the dependence of CO frequencies on density to

deduce the imbalance between the valley densities, and also to determine the m_l/m_t ratio more accurately.

Figure 3 summarizes the density dependence of our CO frequencies. Denoting the difference between the valley densities by $\Delta n = n_Y - n_X$, we rewrite Eqs. (2) and (3):

$$f_{\mathrm{CO},Y}^2 = \frac{h^2}{\pi e^2 a^2}\sqrt{\frac{m_l}{m_t}}(n_{\mathrm{tot}} + \Delta n), \tag{5}$$

$$f_{\mathrm{CO},X}^2 = \frac{h^2}{\pi e^2 a^2}\sqrt{\frac{m_t}{m_l}}(n_{\mathrm{tot}} - \Delta n). \tag{6}$$

The slopes and intercepts of the f_{CO}^2 vs n_{tot} plots give the m_l/m_t ratio and Δn. Concentrating on the Y valley, a least-squares fit of $f_{\mathrm{CO},Y}^2$ data points (circles in Fig. 3) to a line leads to values $m_l/m_t = 5.2 \pm 0.5$ and $\Delta n = (-0.6 \pm 0.4) \times 10^{11}$ cm^{-2}. Note that such a small value of Δn is consistent with the nearly valley-degenerate picture deduced from the existence of the $n_{\mathrm{tot}}/4$ peak in the SdH frequency spectrum [Fig. 2(c)].

The above determination of the m_l/m_t ratio is based on the density dependence of $f_{\mathrm{CO},Y}$ only and does not use the measured $f_{\mathrm{CO},X}$. As a consistency check, we use Eq. (6) to predict f_{CO} for the X valley using m_l/m_t and Δn deduced from the analysis of $f_{\mathrm{CO},Y}^2$ above. This prediction, shown as a dashed line in Fig. 3, agrees well with the measured $f_{\mathrm{CO},X}^2$ (solid squares), and confirms that we are indeed observing COs for both valleys.

We have repeated similar experiments in a sample from a different wafer, containing a 2DES confined to a 15 nm-wide AlAs quantum well. In this sample only the COs of the Y valley could be reliably determined. By performing similar analysis using Eq. (5), in the density range from 5.5 to 9×10^{11} cm^{-2}, we deduce $m_l/m_t \simeq 5.4$, in good agreement with the results presented here.

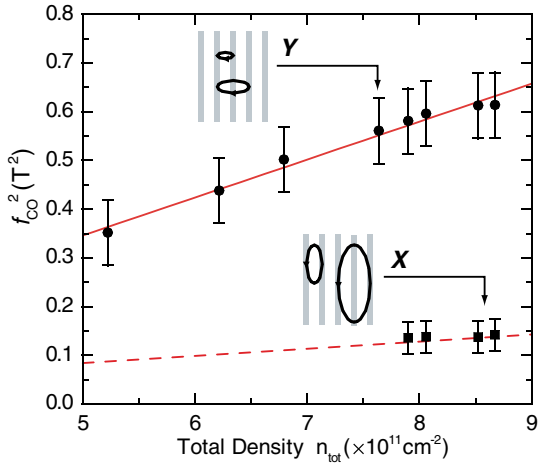

FIG. 3 (color online). Density dependence of the CO frequencies for the Y (circles) and X valleys (squares). The line through the circles is a least-squares fit to the data; its slope determines the ratio m_l/m_t and its intercept the density difference Δn of the two valleys. The dashed line is described in the text.

At this point it is worthwhile emphasizing that the COs described here uniquely probe the m_l/m_t ratio [17]. Conventional experiments that probe the effective mass, such as cyclotron resonance or measurements of the temperature dependence of the amplitude of the SdHOs, lead to a determination of the cyclotron effective mass, m_{CR}. In a 2DES with an elliptical Fermi contour, m_{CR} is equal to $(m_l m_t)^{1/2}$, and therefore provides information complimentary to the m_l/m_t ratio, so that m_l and m_t can be determined. In fact, using the measured $m_{CR} = 0.46m_e$ in AlAs 2DESs [18], we use the $m_l/m_t = 5.2 \pm 0.5$ ratio to deduce $m_l = (1.1 \pm 0.1)m_e$ and $m_t = (0.20 \pm 0.02)m_e$. These values are in good agreement with the (theoretical) value of $m_t = 0.19m_e$ that is calculated in Ref. [17], and $m_l = 1.1m_e$ that is deduced from the Faraday rotation measurements [17]; they also agree well with the results of the majority of theoretical and experimental determinations of the effective mass in AlAs.

We proceed to extract more information, such as the amplitude, phase, and scattering time for the COs of each valley by performing partial inverse Fourier analysis. Figure 4 summarizes the results of such analysis. The Fourier power spectrum shown in Fig. 2(b) is separated into two ranges [19], chosen to isolate the two CO peaks. The range for COs of Y valley ($0.57 < f_{\mathrm{CO}} < 1.21$ T) is inverse Fourier transformed and the result is shown as the solid curve in Fig. 4(a). The range for the COs of X valley ($0.29 < f_{\mathrm{CO}} < 0.57$ T), is analyzed in a similar manner and the result is the solid curve in Fig. 4(b) [20].

We fit the deduced COs for each valley to a simple expression that assumes the amplitude of the COs decreases exponentially with $1/B$:

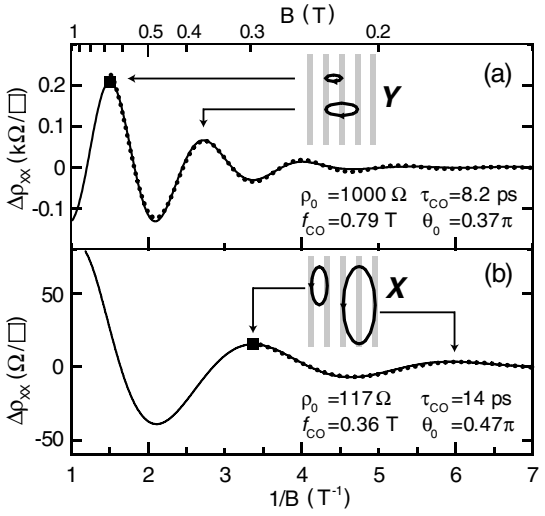

FIG. 4. Results of the inverse Fourier decomposition of the COs of Fig. 2 for the Y and X valleys. The dotted curves show the best fits of Eq. (7) using the indicated parameters. The fits are done only for fields smaller than those marked by square-which indicate the positions of the first CO resonant orbits. The arrows indicate where the first two CO resonance occur.

$$\Delta\rho_{xx} \propto \rho_0 \exp(-\pi/\omega_c\tau_{\mathrm{CO}}) \cos(2\pi f_{\mathrm{CO}}/B - \theta_0), \quad (7)$$

where $\rho_0, \tau_{\mathrm{CO}}, f_{\mathrm{CO}}$, and θ_0 are the fitting parameters; $\omega_c = eB/m_{CR}$ is cyclotron frequency with $m_{CR} = (m_l m_t)^{1/2} = 0.46 m_e$. The exponential term in Eq. (7) is analogous to the Dingle factor used to describe the damping of the SdHOs' amplitude with increasing $1/B$, and has been used successfully to fit COs in GaAs 2D electrons [21] and holes [22]. In Fig. 4 the results of the best fits are shown as dotted curves along with their fitting parameters. The best-fit θ_0 for the COs of Y and X valleys are 0.37π and 0.47π, respectively, in excellent agreement with the expected value of 0.5π (the relative phase errors are 6% and 2% of 2π). This consistency affirms that the reconstructed oscillations faithfully represent the COs of the two valleys. The amplitude of the oscillations for the Y valley is larger than for the X valley as expected from the shorter real-space, resonant orbital trajectories for this valley [Fig. 1(b)]. On the other hand, the scattering times, τ_{CO}, that we deduce from the fits are comparable for the two valleys, suggesting that scattering is nearly isotropic [23]. These τ_{CO} are also comparable to the mobility scattering time, $\tau_\mu \sim 10$ ps, but larger than the quantum lifetime, $\tau_{SdH} \simeq 0.8$ ps, which we deduce from fitting the B dependence of the amplitude of the SdHOs to the damping factor $\exp(-\pi/\omega_c\tau_{SdH})$. The observation that τ_{SdH} is much smaller is not surprising, given that SdHOs are sensitive to all scattering events (both small- and large-angle).

We close by reflecting on possible areas where future ballistic transport in AlAs 2DESs can be applied. One area involves studies of ballistic *spin polarized* currents. Because of the large values of effective mass and g factor [24] of AlAs 2D electrons, it is sufficient to apply an in-plane magnetic field of only a few T to fully spin-polarize the electrons. Such studies are of current interest as they have relevance for spintronic devices. A second area concerns chaotic transport in antidots. The highly anisotropic electron Fermi contours of AlAs 2D electrons should lead to interesting phenomena, examples of which have been reported recently in GaAs 2D hole systems which also possess noncircular Fermi contours [25].

We thank the NSF and ARO for support, and J. J. Heremans and R. Winkler for illuminating discussions.

[1] E. P. De Poortere *et al.*, Appl. Phys. Lett. **80**, 1583 (2002).
[2] Y. P. Shkolnikov *et al.*, Phys. Rev. Lett. **89**, 226 805 (2002).
[3] E. P. De Poortere *et al.*, Phys. Rev. Lett. **91**, 216 802 (2003).
[4] T. P. Smith, III *et al.*, Phys. Rev. B **35**, 9349 (1987); Surf. Sci. **196**, 287 (1988).
[5] H. W. van Kesteren *et al.*, Phys. Rev. B **39**, 13 426 (1989).
[6] K. Maezawa *et al.*, J. Appl. Phys. **71**, 296 (1992).
[7] T. S. Lay *et al.*, Appl. Phys. Lett. **62**, 3120 (1993).
[8] S. Yamada *et al.*, Physica (Amsterdam) **201B**, 295 (1994).
[9] D. Weiss *et al.*, Europhys. Lett. **8**, 179 (1989).
[10] R. R. Gerhardts *et al.*, Phys. Rev. Lett. **62**, 1173 (1989).
[11] R. W. Winkler *et al.*, Phys. Rev. Lett. **62**, 1177 (1989).
[12] C. W. J. Beenakker, Phys. Rev. Lett. **62**, 2020 (1989).
[13] More precisely, as Eq. (1) indicates, a maximum in ρ_{xx} is seen whenever the cyclotron orbit diameter equals $a(p + 1/4)$, where p is an integer. In Fig. 1(b), for simplicity, we schematically show the conditions for the first two resonances as when the diameter is equal to a and $2a$.
[14] The initial 2DES density in our sample at zero front gate bias was 4×10^{11} cm^{-2}; we achieved this density by illumination under a positive back-gate bias [see E. P. De Poortere *et al.*, Phys. Rev. B **67**, 153 303 (2003) for details].
[15] S. K. Mitra and J. F. Kaiser, *Handbook for Digital Signal Processing* (Wiley, New York, 1993), p. 1157.
[16] As detailed in Ref. [2], the spin and valley degeneracies are lifted at higher B, leading to the presence of the $n_{tot}/2$ and n_{tot} peaks in the Fourier spectrum.
[17] Faraday rotation experiments can also determine m_l/m_t, but such determination requires knowing m_l or m_t and the $\langle\tau^2\rangle/\langle\tau\rangle^2$ ratio where τ is the scattering time. In fact, B. Rheinländer *et al.* [Phys. Status Solidi B **49**, K167 (1972)] used Faraday rotation measurements in bulk AlAs and, assuming $m_t = 0.19 m_e$ (determined from a $\mathbf{k}\cdot\mathbf{p}$ calculation) and $\langle\tau^2\rangle/\langle\tau\rangle^2 = 1$, deduced $m_l/m_t = 5.7$.
[18] The most accurate cyclotron resonance (CR) measurements in AlAs 2DESs so far were reported by T. S. Lay *et al.* [7], and yielded $m_{CR} = (0.46 \pm 0.02) m_e$. This value is in very good agreement with the results of CR measurements by N. Miura *et al.* [Solid State Commun. **79**, 1039 (1991)] on n-type AlAs layers [$m_{CR} = (0.47 \pm 0.01) m_e$], and by T. P. Smith III *et al.* [4] on 2DESs in multiple AlAs quantum wells ($m_{CR} \simeq 0.5 m_e$); the latter data, however, show a very broad CR. There was also a CR study of GaAs/AlAs short-period superlattices by H. Momose *et al.* [Physica (Amsterdam) **4E**, 286 (1999)], where $m_t = 0.21 m_e$ and $m_l = 1.04 m_e$ were deduced. For a summary and discussion of AlAs effective masses, see Q. Guo *et al.*, Phys. Status Solidi B **197**, 111 (1996).
[19] Varying these ranges by reasonable amounts (e.g., $\pm 20\%$) leads to rather small ($< \mp 10\%$) changes in the parameters, such as τ_{CO}, that are deduced from the inverse Fourier transform curves.
[20] Subtracting the sum of CO traces of each individual valley (Fig. 4) from the original CO trace [Fig. 2(a)] gives a featureless, nonoscillatory background signal.
[21] J. P. Lu and M. Shayegan, Phys. Rev. B **58**, 1138 (1998).
[22] J. P. Lu *et al.*, Phys. Rev. B **60**, 13 776 (1999).
[23] For a circular cyclotron orbit trajectory, or for an elliptical orbit if we use the average Fermi velocity along the trajectory, the $\exp(-\pi/\omega_c\tau)$ term in Eq. (7) is equivalent to $\exp(-L/2l)$ where L is the orbit length and l the mean-free-path. For the data of Fig. 4, a $\tau \sim 10$ ps corresponds to $l \sim 0.5$ μm.
[24] S. J. Papadakis *et al.*, Phys. Rev. B **59**, 12 743(R) (1999).
[25] M. Zitzlsperger *et al.*, Europhys. Lett. **61**, 382 (2003).